The effect of dodecylbenzenesulfonic acid molecules on poly(4,4-diphenylether-5,5-dibenzimidazole) films

Amir A. Tahrim,[1,2] Laura Crespo,[2] Lourdes Franco,[2,3] Carlos Alemán,[2,3] Elaine Armelin[2,3*]

[1] *University Kuala Lumpur, Malaysian Institute of Chemical and Bioengineering Technology (UniKL MICET), 78000 Alor Gajah Melaka, Malaysia.*

[2] *Departament d'Enginyeria Química, EEBE, Universitat Politècnica de Catalunya, C/ Eduard Maristany, 10-14, Ed. I.2, 08019, Barcelona, Spain.*

[3] *Barcelona Research Center for Multiscale Science and Engineering, Universitat Politècnica de Catalunya, C/ Eduard Maristany, 10-14, Ed. I.S, 08019, Barcelona, Spain.*

***** Corresponding author: elaine.armelin@upc.edu

Abstract

The main aim of the present work was to approach the effect of the addition of an organic acid dopant, dodecylbenzenesulfonic acid (DBSA), in the preparation of poly(4,4-diphenylether-5,5-dibenzimidazole) (OPBI) films, commonly used as proton exchange membranes (PEMs). For this purpose, DBSA was blended with OPBI polymer matrix, at different concentrations, to evaluate the effect of such molecules in the proton conductivity of OPBI membranes. A substantial improvement in the dimensional stability of OPBI film, either for the undoped or for the phosphoric acid doped membranes, with low content of DBSA (12.5 wt.%) was achieved. Moreover, the charge mobility in OPBI/DBSA films remained stable between 22 ºC and 140 ºC, for both doped and undoped states. Therefore, the utilization of OPBI/DBSA system can be envisaged for proton exchange membrane operations at moderate temperature interval.

Keywords: polybenzimidazole; phosphoric acid; proton conductivity, proton-exchange membrane

INTRODUCTION

Proton exchange membranes (PEMs) based on polybenzimidazole (PBI), short name for poly[2,2'-(m-phenylene)-5,5'-bisbenzimidazole], exhibit high proton conductivity, and very high thermal stability.[1–7] Among high performance plastics, PBI is the amorphous thermoplastic polymer with the highest glass transition temperature (of 420-427ºC), with no melting point and a decomposition temperature upper than 500°C.[8] Its excellent thermo-mechanical stability was evidenced by the high heat deflection temperature (HDT, 435°C) obtained at 1.8 MPa, and its particularly high strength in and recovery from compression tests, with compression modulus similar to that of aluminum (5900-6200 MPa).[9] Moreover, the polymer has good chemical resistance and excellent textile fiber properties,[10] being usually employed to fabricate high-performance protective tools, such as synthetic fibers for firefighter's protective clothes, astronaut and welder's suits. In rigid structures, like in aircrafts, it has applications in the cone-shaped nose, which absorbs the landing on impact, minimizing damage, and in the laminated ablative structures of rocket nozzles that require protection in a high thermal environment. Finally, in the form of paste or viscous liquid, it has been employed as adhesive for joints. Currently, there are commercially available products manufactured with undoped PBI polymers in sheet, rod and fibre forms. The semi-fabricated items (rods and sheets) are made, normally by powder sintering processes, like that commercialized by the company Goodfellow Corporation, with brand name of Celazole®.

Nowadays, the most investigated utilization of PBI and its derivatives is in high-temperature polymer electrolyte membrane fuel cell (HT-PEMFC) for energy conversion and storage devices.[3, 5, 8, 11] Development of HT-PEMFCs has open new insights in clean energy alternatives for automotive and stationary power fields.[12–15] Recently, Subianto[4] has reported a list of the main manufacturers of commercially available fuel cell systems with HT-PEMFC components, suggesting that phosphoric acid-impregnated PBI-type polymer

membranes (PBI/PA), *i.e.* PBI membranes doped with phosphoric acid, are the most promising.

One of the most studied PBI derivatives is poly(4,4-diphenylether-5,5-dibenzimidazole) (OPBI),[16–18] in which the presence of aryl ether group (Ar-O-Ar) enhances the flexibility of PBI polymer chain and improves its restricted solubility properties. Nevertheless, undoped OPBI is not a proton conducting polymer and, therefore, for solid electrolyte membrane applications the polymer chains must be doped with acid molecules in order to facilitate the movement of protons across the membrane.[8, 19] The choice such acid affects the maximum proton conductivity properties, the mechanical integrity and the water absorption. Gómez-Romero and co-workers[3] showed that the proton conductivity of acid-doped PBI membranes increases as follows: H_2SO_4 > H_3PO_4 > $HClO_4$ >HNO_3 >HCl. Although the sulphuric acid molecules are the best dopants for PBI,[20] it does not have much use because the membrane requires humidification, similar to the Nafion® PEMs. Therefore, phosphoric acid (H_3PO_4) doped membranes are the most commonly used because of its ability to operate under anhydrous conditions and its thermal stability at temperatures up to 200ºC.[5, 10]

Phosphoric acid (PA) acts as both donor and acceptor in proton transfer and, therefore, allows for proton migration along the anionic chain. Nevertheless, when doped, the membrane mechanical integrity gets much worse, representing one of their major handicaps for the application of doped OPBI in PEMFC devices. Another problem associated with PA dopant molecules is that they can migrate away from the PEM with time, due to the low intermolecular interactions with the polymer matrix. Some studies are proposing alternatives to overcome such drawbacks.[21–27] Moreover, the obtaining of OPBI hybrid materials with better mechanical integrity than OPBI phosphoric acid doped, as for example, by the synthesis of OPBI with other inorganic phosphate derivatives or sulfonic acid derivatives, are another interesting approaches.[28] Jana and co-workers[29] recently reported the use of several acid surfactant molecules as co-dopant molecules for OPBI systems. They have

demonstrated an increased storage modulus and higher proton conductivity (one order higher) than the orthophosphoric acid doped pristine OPBI sample.

Although phosphoric acid doped OPBI-based PEMs have been extensively investigated,[25] it remains a prime challenge to achieve acid co-dopants able to offer superior aforementioned stabilities. In this way, dodecylbenzenesulfonic acid (DBSA) is a good candidate to be tested due to the presence of three chemical structures: (i) long alkyl chain that will impart plasticity to the film; (ii) the aromatic ring that will enhance the miscibility of DBSA with OPBI chains, by π-stacking and van der Waals interactions; and (iii) sulfonic acid that is expected to act as donor and acceptor of protons.

Therefore, in this work we combined the OPBI high thermal stability polymer with the well-known good conductivity of PA inorganic dopant, for either donor and acceptor of protons during conduction, with the help of DBSA molecules. The latter was intended to work as a co-plasticizer compound to increase the flexibility of the whole film, *i.e* as a secondary plasticizer molecule. There are a lot of information about the use of small organic molecules as additives to improve the flexibility of plastics, mostly in PVC,[30, 31]. However, the synergistic effect of secondary molecules as co-plasticizer and in donor/acceptor of protons in PEMs was scarcely explored. Most of the reported works recognizes that some molecules can actuate as co-dopant and co-plasticizer agents, like imidazoles, 1-Methyl-3-propylimidazolium dihydrogen phosphate,[3] or ionic liquids.[32, 33] Therefore, this study will provide new knowledge on such field.

MATERIALS AND METHODS

Materials

For the synthesis of OPBI, 3,3',4,4'-tetraaminobiphenyl (TAB), 4,4'-oxybis (benzoic acid) (OBA) and orthophosphoric acid (PA, 85% H_3PO_4) were purchased from Sigma Aldrich. OPBI was synthesized in our laboratory using the procedure described below and adapted from previous work.[17] Ammonium hydroxide solution (28% NH_3 in water), formic

acid (FA, 98%), and dodecylbenzenesulfonic acid (≥95%, DBSA) were also purchased from Sigma Aldrich. All chemicals were used as received. All other reagents, unless otherwise specified, were of analytical grade and were used as received.

Synthesis of OPBI neat polymer and OPBI/DBSA films

For the OPBI synthesis, 2.20 g (8.5 mmols) of TAB and 1.82 g (8.5 mmols) of OBA were mixed with PA and placed in 250 mL three-necked round bottom flask equipped with reflux condenser with an inlet of nitrogen gas flow.[17] The reaction mixture was stirred with a mechanical overhead stirrer (50 rpm) and a slow stream of purged nitrogen gas (0.55 bar) was maintained throughout the reaction. Then, the mixture was placed in an oil bath and the temperature was controlled with a temperature controller at 190-220 ºC for 26 h. The reaction mixture became more viscous and a dark brown colour solution appeared at the end of the polymerization time. The brown colour belongs from the phosphoric acid molecules, that are necessary to prepare the polymer. After this, the mixture was poured into a beaker with double-distilled water and a brown powder precipitated. The mass was pulverized and neutralized with sodium bicarbonate (5%), washed thoroughly with water, and finally dried in a vacuum oven for 24 h at 100 ºC to obtain the dry OPBI powder. Although the powder is neutralized, some molecules of PA is still trapped inside the polymer matrix to impart proton-exchange properties to such material. Therefore, it will be evidenced in the characterization results of undoped OPBI films.

In order to prepare OPBI neat membranes, 10% of OPBI solution in a small sample container, approximately 200 mg of OPBI powder were weighted. By using a micropipette, 2 mL of FA were added into the flask. The solution was then placed in a water bath at 40 ºC

and stirred with a magnetic stirrer until complete dissolution. Since the OPBI powder was dissolved, the solution was poured onto a glass Petri dish to cast the membrane after the acid-water evaporation. For this step, the Petri dish was covered with permeable paper and left under fume hood at room temperature overnight. After the drying process, the OPBI film was peeled out from the Petri dish and stored in a glass container and desiccator for further use.

In order to get OPBI films with mechanical integrity to be manipulated, DBSA was used as co-dopant and co-plasticizer agent. The influence of DBSA in the PA doping process was studied considering several concentrations of the former (50 wt. %, 37.5 wt. % and 12.5 wt. %, with respect to polymer concentration: 20 mg/8 mL of FA). The mixtures of OPBI and DBSA, in FA, were left to heat at 40 ºC until homogenization. After that, the film casting was carried out applying the procedure that previously described for OPBI neat membranes.

Doping process

For the obtaining of PA-doped OPBI membranes, dried films were immersed in a solution of 85% PA (11 M) for 7 days. After this period, membranes were taken out from the acid viscous liquid using thongs and the residual solvent was wiped off with a filter paper. After that, samples were stored in a desiccator under vacuum conditions. Then, the polymer films were dried at 110 ºC under vacuum until unchanged weight was reached. The PA doping level of all the OPBI nanocomposite membranes were determined by weight, in percentage, before and after the doping process. The results were expressed according to the water uptake and swelling methods described in the ESI.

Physical-chemical characterization

Fourier-transform infrared (FTIR), Raman and nuclear magnetic resonance (NMR) spectroscopies were employed for the structural characterization of the powders and polymeric films. The FTIR spectra were measured in the range of 600-4000 cm^{-1} with a FTIR 4100 Jasco spectrophotometer coupled to an attenuated total reflection (ATR) accessory with a diamond crystal (Specac model MKII Golden Gate Heated Single Reflection Diamond ATR). Raman spectra were obtained through Renishaw InVia confocal Raman microscope, with a laser excitation source of 785 nm, an exposure time of 1 s, a laser power of 0.1%, 3 accumulations and with the Raman shift range of 600-1800 cm^{-1}. For both spectroscopic studies samples consisted of solid films of approximately 3×3 mm^2 area, with the exception of OPBI neat polymer, which was a powder. The chemical structures and the acid doping state of the OPBI and OPBI/DBSA were determined by ^{13}C-NMR and ^{31}P-NMR spectroscopy using a Bruker NMR Ascend 400 spectrometer (400 MHz), equipped with two probes for a liquid and solid samples. Samples were finely mortared and were used in solid state. A solid standard bore probe was used to calibrate the equipment for experiments with routine solids. Pure amino phosphoric acid (H_6NO_4P) was used as an internal standard for the doped acid films. The experiments were conducted at 20ºC.

The chemical composition of OPBI homopolymer and OPBI modified films was determined by X-ray photoelectron spectroscopy (XPS). XPS analyses were performed in a SPECS system equipped with a high intensity twin anode X-ray source XR50 of Mg/Al (1253 eV/1487 eV) operating at 150 W, placed perpendicular to the analyzer axis, and using a Phoibos 150 MCD-9 XP detector. Samples were fixed mechanically into a special sample holder using a double side tape. The spectra were recorded with a pass energy of 25 eV in

0.1 eV steps at a pressure below 6×10^{-9} mbar. The C 1s peak, with a binding energy of 284.8 eV, was used as an internal reference. The atomic percentage of the main elements (C 1s, O 1s, N 1s and S 2p) was determined by dividing the peak area of the most intense XPS signal of each element by the corresponding sensitivity factor and expressing it as a fraction of the sum of all normalized peak areas. The area of analysis was at about 3 mm^2. High resolution XPS spectra were acquired by Gaussian/Lorentzian curve, fitting after S-shape background subtraction, for the following elements: C 1s, O 1s, N 1s and S 2p.

The analysis of the cryo-fractured surfaces of OPBI and OPBI/DBSA films, was conducted by scanning electron microscopy (SEM) using a Focus Ion Beam (FIB) Zeiss Neon 40 instrument (Carl Zeiss, Germany) operating at 5kV, equipped with an EDX spectroscopy system. Films were covered with conductive carbon coating using Mitec K950 Sputter Coater before SEM analysis.

Thermogravimetric analysis (TGA) was carried out with a TG SETSYS 12 Evolution of SETARAM, equipped with Setsoft 2000 software, for SETARAM Thermal Analysis Systems. Experiments were conducted at a heating rate of 10ºC/min, under argon atmosphere, from 25ºC to 1100ºC. The polymer mass required for this experiment was at about 15 mg.

Contact angle measurements were performed by employing an OCA 20 (DataPhysics Instruments GmbH, Filderstadt) equipment and using the sessile drop method at room temperature. For the static contact angle (sCA) measurements, 0.500 μL droplets of distilled water were dispensed on the respective film surfaces (flat films with 1.5×1.5 cm^2 of area).

The contact angle values were obtained using the software SCA 20 and consisted of the average of, at least, ten independent measures for each sample.

The water uptake and swelling measurements were described in the supporting information (ESI).

Through- plane proton conductivity measurements

The bulk proton conductivity of membranes studied in this work was measured in a through plane cell, composed by two-electrodes of stainless steel, with AC impedance method (electrochemical impedance spectroscopy, EIS), over a frequency range of 10^4 Hz to 10^{-2} Hz, 10 mV of amplitude for the sinusoidal voltage, on an AUTOLAB-302N potentiostat/galvanostat. The volume of the cell is defined by a 15 mm inner diameter and a 2 mm inner depth. The pressure is kept constant and defined by the maximum limits of screws used to close the probe arrangement. For such assays, films were previously cut into disks of about 15 mm of diameter; and the dry film thickness (DFT) values were measured for each film, with a Neurtek Mega-Check pocket FE device. Experiments were conducted at five different temperatures, 22ºC, 100ºC, 140 ºC, 160 ºC and 180 ºC. As the absorbed humidity of the membranes should be totally eliminated before the conductivity measurements, we kept the membranes in the oven at 100ºC before putting them into the conductivity cell, to ensure the low humidity conditions. After that, the whole system was kept at the desired temperature until stable value. Then, the proton conductivity values as a function of variable temperature were recorded during the cooling process. In the case of the OPBI/DBSA doped membranes, these were dried at 100°C by heating and holding at 100°C isothermally for 2 h to remove the water from the membrane, before carrying the high temperature experiments.

In an effort to keep the samples dried and under humidity control, membrane samples were cooled in a vacuum oven and taken out immediately before the conductivity measurements. The bulk resistance of the films (R_b), in ohms (Ω) was obtained from the Randles circuit, measured from impedance plots. The conductivity was calculated with the following equation:

$$\sigma = \frac{L}{R_b A} \qquad (Eq.1)$$

where, σ is the proton conductivity (S/cm), L is the distance between the two probes of the capacitor cell (fixed to 0.20 cm), A is the area of the electrodes in the case of the through-plane setup (in cm^2).

RESULTS AND DISCUSSION

Preparation of OPBI/DBSA films

Since the high glass transition temperature of OPBI precludes the utilization of conventional melt-processing techniques, films were prepared using casting procedure. Observing the casted films (Figure 1), the presence of DBSA in the undoped OPBI matrix seems to do not affect the homogeneity of the OPBI membrane. Figure 1a shows that with the highest DBSA content (50 wt. %), the film adhered to the Petri dish has some brittle behavior. The OPBI/DBSA film with a moderate concentration of DBSA molecules (37.5 wt.%) exhibits good integrity (Figure 1b). Finally, films obtained with 12.5 wt. % DBSA (Figure 1c) are very flexible and can be detached easily from the glass container, in the undoped state. According to these results, hereafter additional studies were only conducted using the lowest DBSA content to avoid fragility and abrupt changes in the thermal properties of OPBI homopolymer.

After doping with PA molecules, all OPBI/DBSA films become flexible and ease to manipulate, confirming that DBSA molecules actuate as a secondary plasticizer additive in OPBI PEMs.[32] The plasticizer effect is caused by the increase of soft segments (*i.e.* the methylene groups in DBSA molecules) to the restricted OPBI backbone (*i.e.* derived from the aromatic rings).

Figure 1. OPBI transparent films with different content of DBSA molecules: a) OPBI/DBSA (50 wt. %); b) OPBI/DBSA (37.5 wt. %); c) OPBI/DBSA (12.5 wt. %).

Structural characterization of pristine OPBI and OPBI/DBSA films

From the FTIR and Raman spectra, it was possible to underscore the appearance of absorption bands assigned to C=C stretching from aromatic ring, C=N stretching and C-H vibration of imidazole moieties, that correspond to the main groups in PBI polymer chains. In addition, undoped and doped films exhibit broad absorption bands that correspond to the PA molecules, proving that the dopant was entrapped inside the OPBI matrix (Figure S1). However, in the doped films there is a great increase on P-OH and P=O interactions by hydrogen bonds and the absorption bands are much more intense than in the undoped films.

The FTIR spectra of OPBI films with 12.5 wt.% of DBSA are shown in Figure 2. The peaks at 3393, 2916, 1031 and 1006 cm^{-1} have been assigned to O-H stretching, C-H stretching of $–CH_2$, S=O stretching and >CH stretching of benzoic rings in both OPBI and DBSA components, respectively. The S=O and C-S stretching from DBSA were reported to appear at 1043 and at 834 cm^{-1}, respectively. Some of those peaks were hardly observed in

the doped films due to the overlapping with the absorption bands of PA in the wavenumber regions comprised between 3000-2500 cm^{-1} and 1200-500 cm^{-1}.

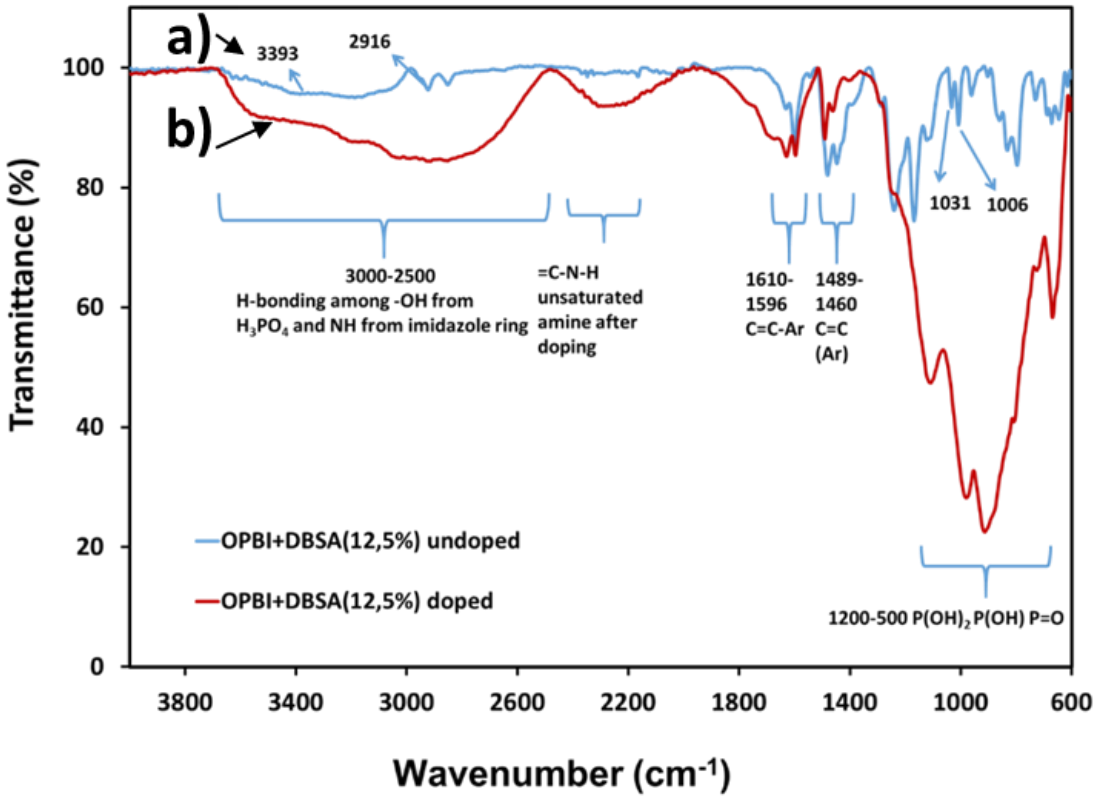

Figure 2. Infrared spectra of: a) undoped OPBI/DBSA (12.5 wt. %) and b) PA-doped OPBI/DBSA (12.5 wt. %) films.

Although the Raman spectrum of pure PBI was already described,[10, 34] Raman studies on OPBI films modified with sulfonic acid molecules are scarce. In the present work, we used Raman spectroscopy to study the nonpolar absorption bands of OPBI films and the changes caused by doping with PA. The Raman spectra of undoped and doped OPBI pristine membranes are displayed in Figure 3, while the Raman spectrum of undoped and doped OPBI/DBSA (12.5 wt.%) films is shown in Figure S2, respectively. The peaks at 1616, 1577 and 1548 cm^{-1}, which are assigned to the C=C stretching of aromatic moieties, represent the most intense bands in the Raman spectra of undoped membranes. The last peak (1548 cm^{-1})

and the one at 1460 cm^{-1} could also be assigned to the C=N stretching, whereas the peak at 964 cm^{-1} could be assigned to C-H deformation of benzene ring.[10] In comparison with those for the undoped film, the spectra recorded for the doped one (different zones in the optical images, Figure 3, inset) show wider and broader absorption bands between 1250-1397 cm^{-1} than the undoped films, as expected. Those absorption bands come from P=O vibrations when stablishing hydrogen bonds among them and with the polymer matrix. The intense peak at about 960 cm^{-1} is usually attributed to P-OH vibrations but also overlaps with the C-H vibrations of benzene ring. The Raman spectrum of pure PA is provided in Figure S3, where pure P-OH signals at 911cm^{-1} can be seen.

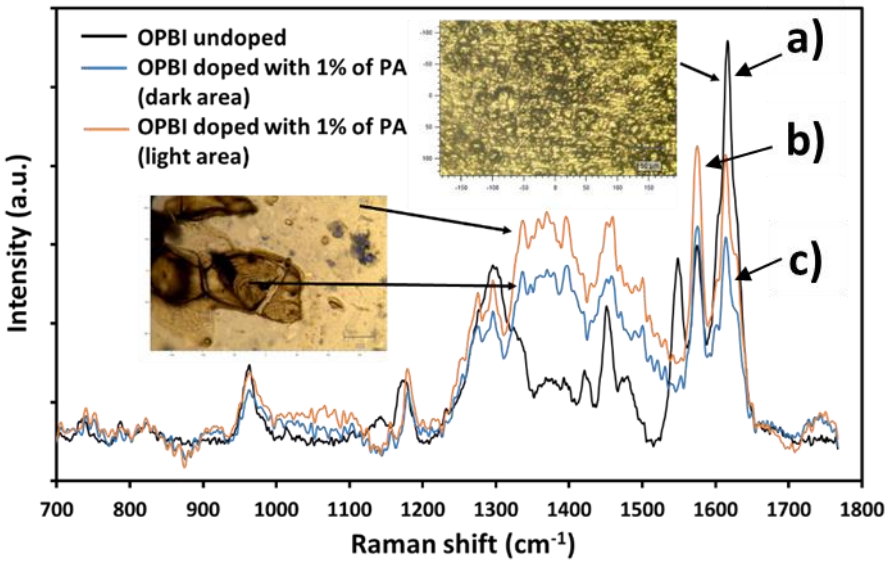

Figure 3. Raman spectra of: a) undoped OPBI; b) PA-doped OPBI (light zone on optical micrograph; and c) PA-doped OPBI (dark zone on optical micrograph) films. Images correspond to the optical micrographs of different zones approached above the samples surfaces.

Additionally, to FTIR and Raman spectroscopy characterizations, solid-state ^{13}C-NMR was used to elucidate the structure of the polymer backbone and its interaction with the

DBSA molecules. Figures 4a-b display the spectra recorded for pure and undoped OPBI and OPBI/DBSA (12.5 wt. %), respectively. As it can be seen, there are several notable differences between both compounds. The main peaks from pristine polymer, which are located at the chemical shift of 100-160 ppm, are attributed to the benzene and imidazole rings. Our results are in good agreement with previous studies reported [17, 29, 35–37] as well as with the theoretical chemical shift calculated for carbon.

By contrary, in the OPBI/DBSA compound (Figure 4b), the chemical shift from methyl and methylene units of DBSA was easily identified among 14 ppm to 40 ppm. The peak at δ 14.8 ppm is from a terminal CH_3, and the peak at 23.5-47.9 ppm is from intermediate CH_2 groups of the alkyl chain. Surprisingly, a single resonance signal can be detected at 176 ppm, which is unambiguously attributed to residual FA trapped inside the polymer matrix. On the other hand, the chemical zone related to the benzene and imidazole rings is split in comparison to the pristine polymer (Figure 4a). The reason for this effect is the neighbourhood differences between the phenyl C=C of DBSA and the C=C from the aromatic rings of OPBI. Since the aromatic rings shield each other, the absorption frequency as well as the chemical shift can be displaced in the NMR spectrum. However, in this study, chemical shifts of the peaks to up fields were not observed.

The films were prepared in solution of 85% of PA and, subsequently, they were fully doped with the same acid for 7 days. Then, the presence of phosphorous linkages in either undoped or doped films should be detected. The solid-state ^{31}P-NMR was necessary to compare the changes occurred between the doped and the undoped systems. Chemical shifts were referenced by recording a spectrum of neat PA, which was taken as the position of 0

ppm. Both undoped membranes, OPBI and OPBI/DBSA (12.5 wt. %), exhibited the typical PA resonance peaks (Figures S4a-b). Jayakody *et al*.[38] used solid-state ^{31}P NMR to show that the proton diffusivity in PBI matrix is strongly dependent on the membrane processing. According to them, the presence of ^{31}P signals at -14 ppm and -30 ppm is assigned to dimers from pyrophosphoric acid ($H_4P_2O_7$) and from phosphate oligomers (*i.e.* compounds with higher molecular weight than dimers) trapped inside the polymer matrix. Such compounds are the responsible for the mechanism of proton mobility in PBI membrane. The presence of transesterification of phosphoric units is proportional to an improved conductivity in PBI membranes. Therefore, undoped OPBI (Figure S4a) presents more PA trapped than undoped OPBI/DBSA, (Figure S4b), as is reflected by the appearance of a broader resonance and additional peaks (2.6 ppm and -5.4 ppm) in the spectrum of the latter. However, no evidence of PA dimerization or oligomerizations was detected (data not shown). In contrast, the fully doped system (Figure S4c) exhibits the highest PA/OPBI ratio, PA oligomers and dimers being also detected.

Both ^{13}C- and ^{31}P-NMR results support that OPBI membranes are well compounded with the DBSA molecules, and doped with different PA species, necessary for the good conductivity performance of the films.

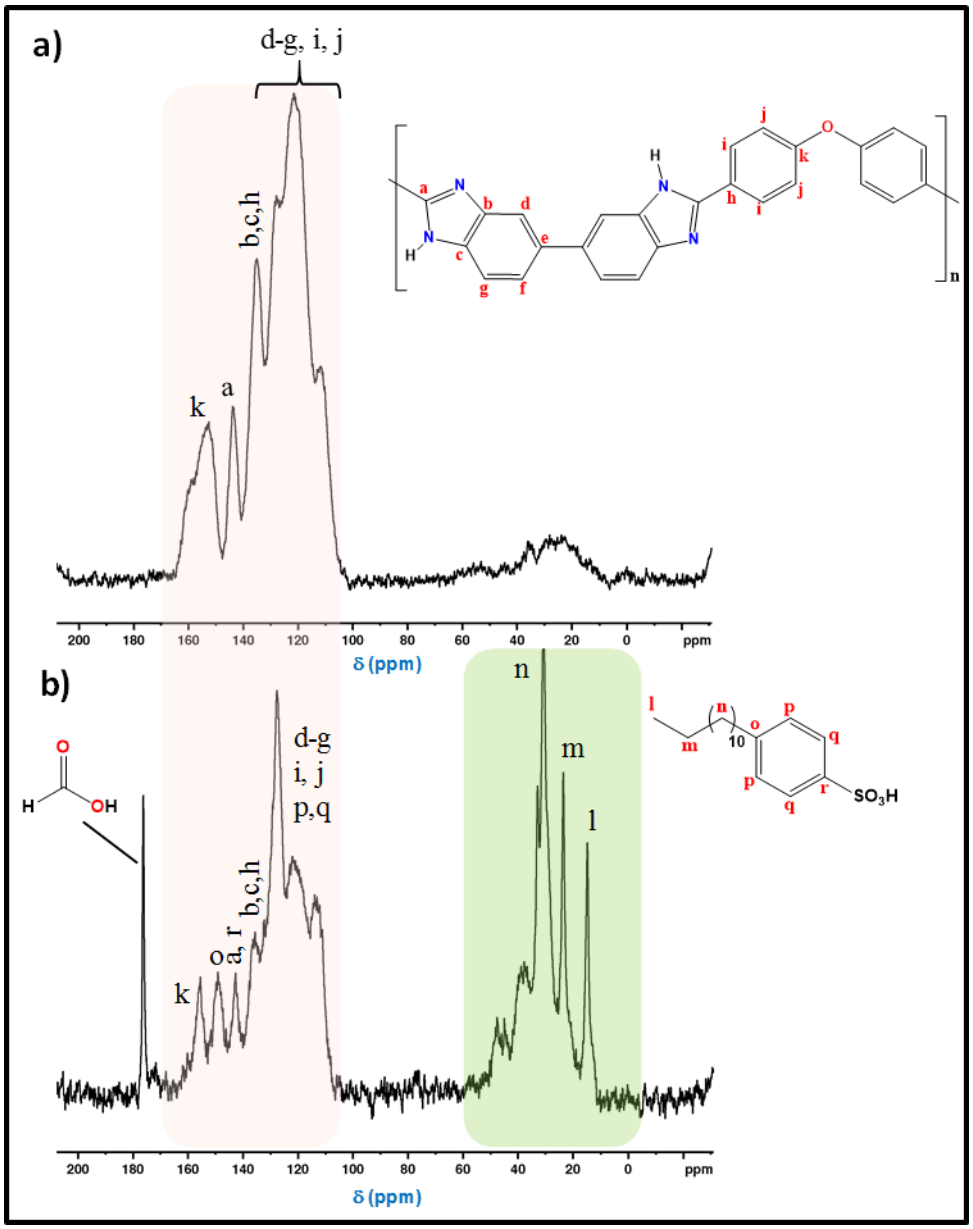

Figure 4. ^{13}C Solid-state NMR of: a) undoped OPBI pristine film and b) undoped OPBI/DBSA (12.5 wt. %) film.

The well incorporation of DBSA molecules to OPBI membranes were further verified by the XPS analysis (Figure 5). The atomic percentages of C, O, N and S are reported in Table 1. As can be seen, the gradual increase in the C/O ratio for OPBI/DBSA compositions can be explained by the increase content of methylene groups from dodecyl chain and from the aromatic ring. The C/O values obtained were 1.16, 1.75 and 2.51, for 12.5 wt. %, 37.5

wt. % and 50 wt. %, respectively. In the same way, the content of S atoms has been increased with high DBSA concentrations, as expected. Compared to the C and O atoms, peaks of either S or N elements are difficult to distinguish in the survey spectra. However, they were better identified with the high resolution spectra included in the supporting information (Figures S5-S8).

Table 1. Atomic concentration (%) of C, O, N and S, determined by XPS analyses for samples studied in this work.

Sample	**C *1s***	**O *1s***	**N 1s**	**S *2p***
OPBI homopolymer	57.8	38.4	3.8	0.0
OPBI/DBSA 12.5 wt.%	51.4	44.4	2.5	1.7
OPBI/DBSA 37.5 wt.%	60.6	34.7	1.7	3.0
OPBI/DBSA 50.0 wt.%	67.0	26.7	2.9	3.4

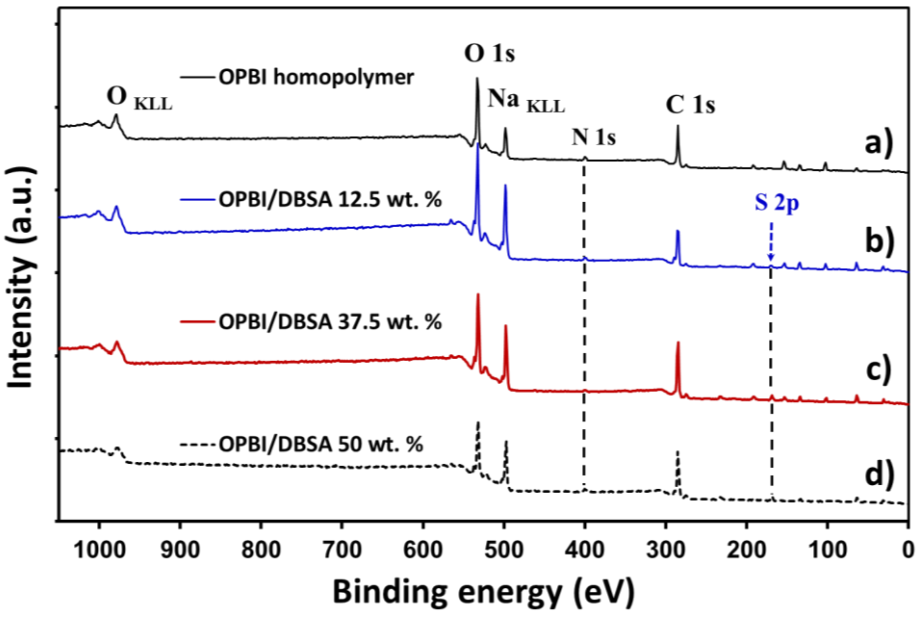

Figure 5. XPS survey spectra of: a) OPBI pristine film; b) OPBI/DBSA (12.5 wt. %); c) OPBI/DBSA (37.5 wt. %); and d) OPBI/DBSA (50 wt. %) modified films.

Influence of DBSA on the thermal stability of OPBI membrane

Regarding the thermal properties, acid doped polybenzimidazoles (PBIs) are familiarly known by their high thermal stability. The effect of adding DBSA acid (12.5 wt. %) on the thermal decomposition of pristine OPBI membrane is visualized in Figure 6, where the undoped OPBI pristine sample is represented on Figure 6a and undoped OPBI/DBSA (12.5 wt. %) is shown in Figure 6b. Three main decomposition processes are clearly distinguished (I, II and IV), considering that decomposition step (I) is related to solvent evaporation. Therefore, pure OPBI homopolymer has two initial weight loss processes. The first process starts below 100ºC and is related to the evaporation of residual water molecules trapped inside the polymer matrix, while the second extends from 100ºC to 200ºC and can be assigned to CO_2 decomposition from terminal carboxyl groups.[6] The polymer chain decomposition occurs between 500ºC to 765ºC, as is evidenced by the sharp weight loss decay. It should be emphasized that the pristine OPBI film is the polymer with the highest decomposition temperature.

The high content of DBSA molecules slightly decreased the chemical stability of OPBI polymer. OPBI/DBSA (12.5 wt.%) exhibits two main degradation steps (Figure 6b: III and IV), the largest temperature decomposition range (460-795ºC), and the lowest value of char yield at 1000ºC (23 %). Although the thermal stability is slightly reduced for this sample, its thermal profile is still good if compared with other thermoplastics. The thermal data are listed in Table 2.

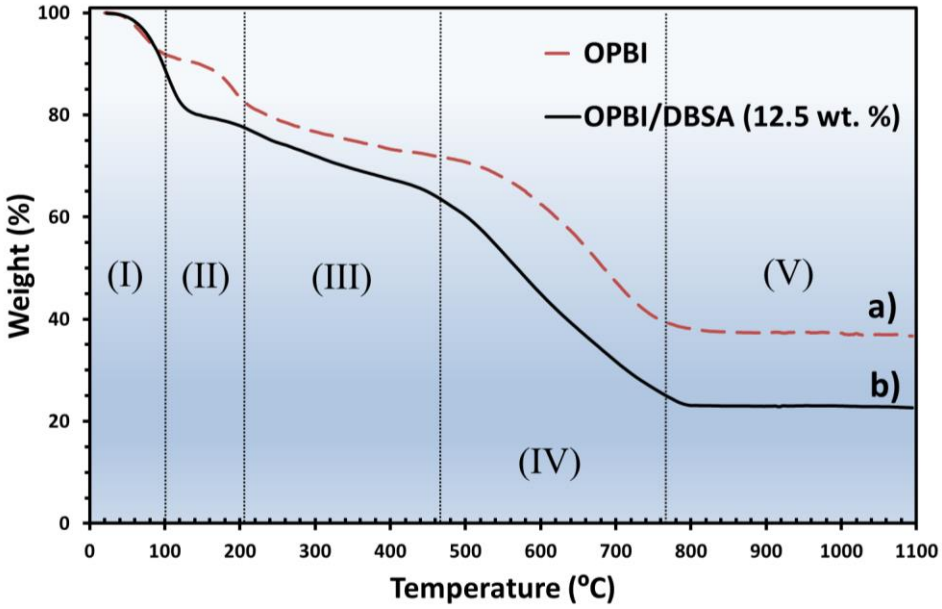

Figure 6. TGA curves of: a) pristine OPBI membranes and b) OPBI samples modified with DBSA molecules (12.5 wt. %). The inset roman numbers correspond to the different transitions observed with increasing temperature.

Table 2. Thermal and wettability properties, and dimensional stability data for OPBI and OPBI/DBSA 12.5 wt. % films.

Property	OPBI	OPBI/DBSA (12.5 wt. %)
$T_{d,0}$ [a] (°C)	500	460
$T_{d,max}$ [b] (°C)	633	628
Char-yield (%)	37	23
WCA [c] (°)	33.5 ± 5.1 (bd)	65.7 ± 4.3 (bd)
	20.3 ± 6.0 (ad)	47.3 ± 6.1 (ad)
Water uptake[d] (%)	8.94 ± 1.29 (bd)	3.07 ± 0.70 (bd)
	- [e]	28.08 ± 4.08 (ad)
Swelling ratio[f] (%)	19.36 ± 4.08 (bd)	1.63 ± 0.91
	28.08 ± 4.08 (ad)	2.20 ± 0.53
Swelling volume[g] (%)	30.32 ± 7.70 (bd)	9.41 ± 1.76 (bd)
	60.71 ± 13.16 (ad)	47.93 ± 7.10 (ad)

a) Temperature of the initial polymer weight loss based on the TGA data at 10ºC/min; b) Temperature of the maximum decomposition peak based on the TGA data at 10ºC/min, c) Water contact angle average after 10 measurements of static water droplet (bd: before doping, ad: after doping with PA for 7 days). d) Values obtained from Equation S1. e) The water uptake from pristine OPBI doped with PA was not possible to measure due to the poor mechanical property of the film after doping. f,g) Values obtained from Equations S2 and S3, respectively.

Effect of DBSA molecules on the OPBI membrane swelling properties

OPBI sample is highly hydrophilic and has high affinity for moisture due to the tendency of –NH and acid groups to form hydrogen bonds with water molecules.[16] The wettability on solid surfaces is governed by three main parameters: the liquid-repellent properties of the compounds onto surface, the surface topography and the roughness. As expected, all studied films were hydrophilic, displaying water contact angles lower than 90º due to the presence of the above mentioned polar groups. However, samples modified with the organic acid molecules, experienced a reduction in such affinities (Figure 7). In this study, one hypothesis of such behavior should be a slight decrease in the number of polar groups at polymer surface and the changes observed in the surface topography (discussed in the next section). It is noticeable that the doping of films with PA results in a decrease of the average contact angle by 20-30 % in each case, reflecting that the surface becomes more hydrophilic (Table 2).

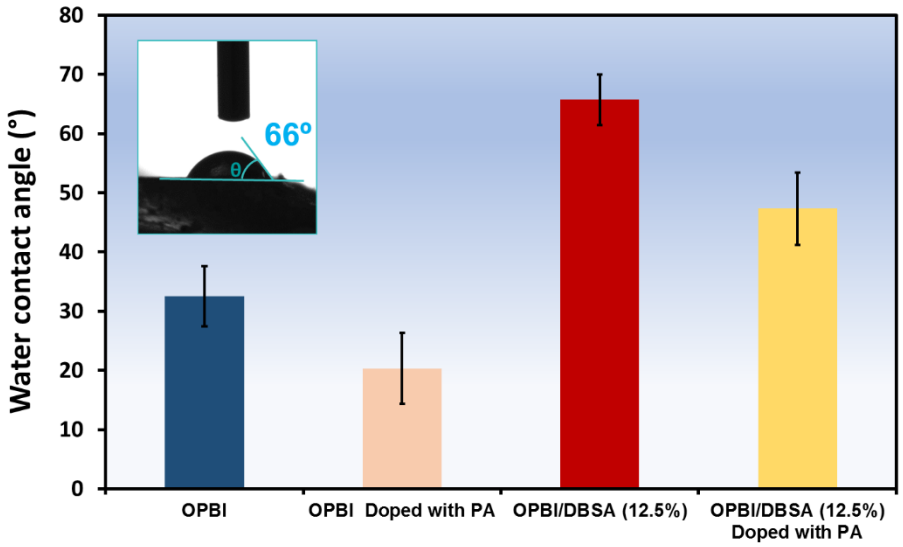

Figure 7. Water contact angle of OPBI neat polymer and OPBI/DBSA films, before and after doping with phosphoric acid (PA). The inset image includes the example of one drop deposited onto undoped OPBI/DBSA (12.5 wt. %) film surface and its WCA calculation (θ).

After immersion of the membrane in distilled water for 3 days, it was found that OPBI can absorb ~9% of water with respect of the dry membrane, whereas OPBI/DBSA only absorbs ~3% (Table 2). However, after complete doping of OPBI/DBSA with PA, a water uptake of 28% (almost ten times higher than the undoped membrane) was obtained, indicating a good capability for acid diffusion across the membrane, even after the incorporation of OPBI compound with DBSA molecules.

Data reported in Table 2 indicates a reduction in the swelling ratio and swelling volume capacities of compounded films with respect to pristine OPBI. However, cross-section FE-SEM micrographs of OPBI/DBSA (12.5 wt.%) reveals a very compact morphology for this samples, even in the doped state (Figure S9). In fact, OPBI samples have more defects than OPBI/DBSA film, which would be an explanation for why the water uptake was not possible to measure in such sample, whereas OPBI/DBSA is stable after doping.

In general, the OPBI samples doped in its two varieties, absorb greater quantity of phosphoric acid molecules than its undoped counterparts do. As for example, comparing the OPBI/DBSA undoped and doped swelling volume, the latter has been increased by a factor of five (Table 2). Therefore, to conclude, OPBI/DBSA (12.5 wt.%) seems to have the good solvent swelling properties to be used as PBI-based fuel cell membrane.

Topography and cross-section analyses of pristine OPBI and OPBI/DBSA films

The morphology and semi-quantitative composition of OPBI films were evaluated with FE-SEM and EDX analyses (Figure 8). At first glance, the pseudo-spheres that appear in the micrograph of undoped OPBI (Figure 8a) were due to the fast evaporation of solvent during the film processing. They are located uniquely on the surface and not inside the film (Figure

S9). The atomic composition for this sample, as observed by EDX analysis, mainly corresponds to C, O and P atoms (Figure 8b). When the membrane is doped (Figures 8c-d), the film becomes flat and smooth in its appearance. The doping process was performed with PA (85%) for 7 days, explaining the increment in the concentration of phosphorous atoms in all doped films with respect to the undoped ones.

Furthermore, the surface of OPBI/DBSA (12.5 wt. %) is shown in Figures 8e-h. As observed, the surface of this sample is heterogeneous before doping, exhibiting darker and clearer zones. EDX analysis proved that the plasticizer is localized in the bright spots due to the detection of sulphur atoms (Figure 8f). When doped, once again the heterogeneity reduces (Figure 8g) and the P concentration (Figure 8h) increases in intensity with respect to the undoped film. In general, SEM studies confirm that the films were well doped, which is agreement with previous spectroscopy characterization results.

The cryo-fracture FE-SEM analysis of OPBI membranes provides understanding about the compactness and homogeneity of the films. Moreover, it also offers some qualitative information about the mechanical integrity of the films (brittle fracture). OPBI/DBSA samples did not exhibit fissures, after the cross-section cut (Figures S9a), and the film seems to delaminate by layers (Figure S9b). Moreover, OPBI/DBSA membrane shows good homogeneity and compactness. Comparison of the crack propagation of undoped and doped films indicates that the doping process improved the mechanical integrity of the films (Figures S9c), none delamination is observed after doping; making them more stable for the swelling experiments. In the case of OPBI/DBSA samples, the crack propagation starts on the top and stops close to the top surface (Figure S9c). A deeper discussion regarding the crack propagation of this sample is provided in the Supplementary Information.

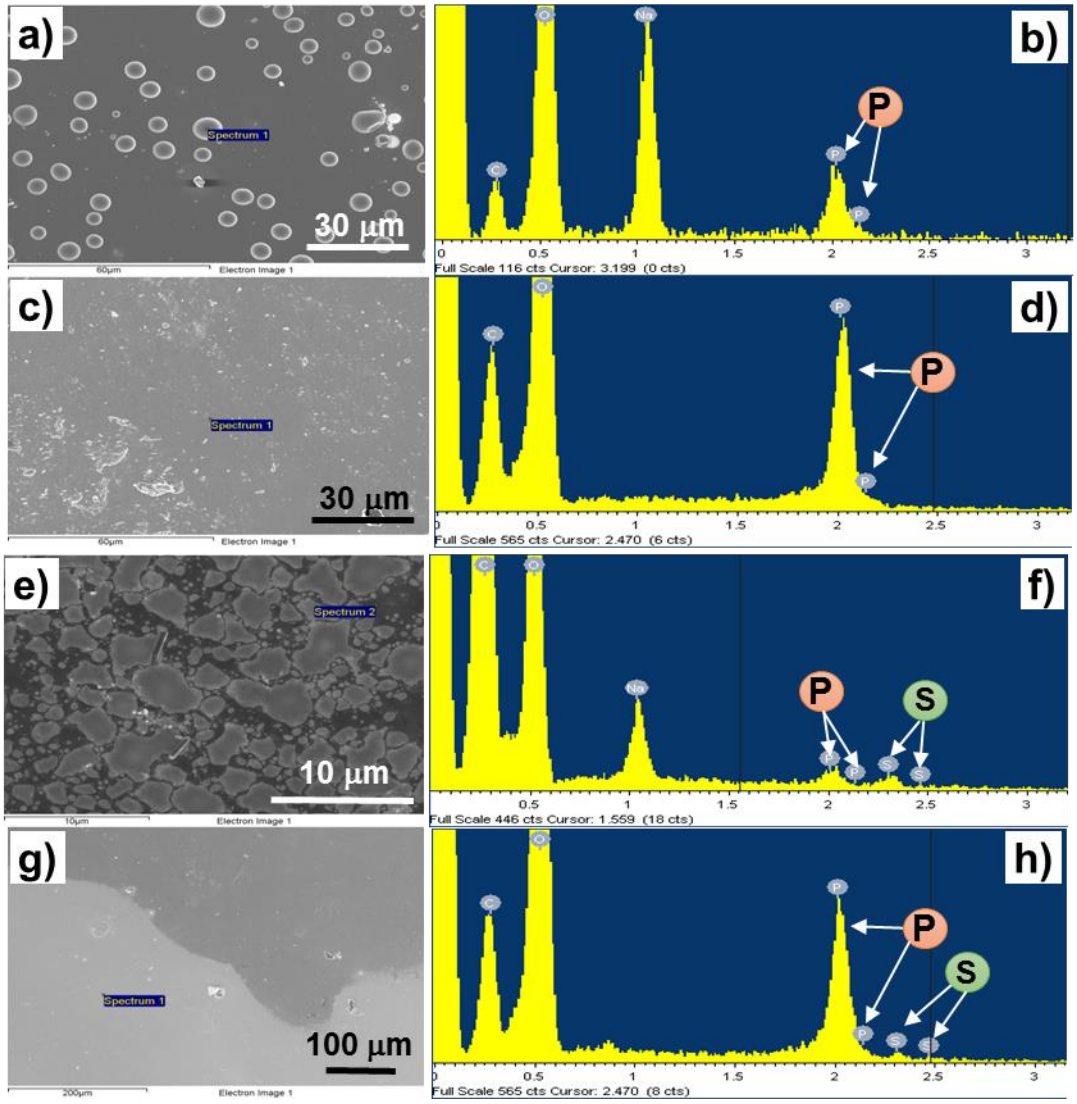

Figure 8. FE-SEM micrographs (on left) and EDX spectra (on right) of the prepared OPBI membranes: (a-b) undoped OPBI; (c-d) doped OPBI; (e-f) undoped OPBI/DBSA (12.5 wt.%); (g-h) doped OPBI/DBSA (12.5 wt. %).

Proton conductivity properties of OPBI/DBSA films

The proton conductivity is an important property in defining the performance of a PEM. This property is directly correlated with the number of proton carriers and their mobile behaviour, which are also dependent on the temperature and acid doping level.[39] The impedance spectroscopy is the most widespread method used for it, where analysis of a

complex-plane frequency dependent response of a sample may allow estimation of sample proton conductivity. The proton conductivity of HT-PEM is usually measured by using in-plane four-probe[40] or two-probe methods[41–43] and is strongly dependent on the cell geometry. In this work, we employed a through-plane cell, with two-electrode configuration and solid membrane impregnated with the acid dopant molecules to measure the bulk resistivity (R_b) of the material, by following the work published by Holdcroft and co-workers.[44] The cell configuration is shown in Figure 9a.

The proton conductivity of the two membranes was measured from 180 ºC to 22 ºC, under anhydrous conditions. Specifically, the humidity absorbed by the membranes was totally eliminated before the conductivity measurements by keeping them into an oven at 100 ºC for 2 h. After this, the membranes were conditioned to the highest temperature of probe and put into the conductivity cell and the system was kept at the desired temperature until stabilization. Then, proton conductivity values as a function of temperature were recorded, as explained in the experimental procedure.

Pristine OPBI and OPBI/DBSA (12.5 wt. %) membranes in both undoped and doped states are compared in Figures 9b-c, while values are summarized in Table S1. As it was expected, the conductivities of doped membranes were perceptibly affected by the temperature and, in addition, the behavior of the two systems was clearly different. The conductivity was found to increase when the membranes passed from 180 ºC to 140 ºC, being the late the highest value found for OPBI doped films (66.9 $mS \cdot cm^{-1}$). By contrary, OPBI undoped films offered the lowest charge mobility in dry conditions at the same temperature (0.088 $mS \cdot cm^{-1}$, Figure 9b). Therefore, the high content of PA trapped inside the doped

polymer matrix led to conductivities significantly higher than those obtained for undoped films (Figure 9b). On the other hand, OPBI membranes modified with DBSA molecules experienced a slightly decrease on the proton conductivity at temperatures comprised among 180 ºC and 100 ºC, in the undoped state (Figure 9c). However, in doped state the behavior was the opposite than OPBI pristine polymer, i.e. the conductivities slightly increase with cooling process, being the maximum value that obtained for the membrane operating at 22 ºC (0.63 $mS \cdot cm^{-1}$, Figure 9c). The possible explanation for such reduction of ionic conductivity with increase temperature can be associated to the decomposition of DBSA at high temperatures and/or to the migration of the co-dopant molecules outside the polymer matrix. The conductivity values reported in this work are consistent to those determined for OPBI membranes, where the acidic surfactant molecules where composed by camphorsulfonic acid (CSA) and *p*-toluenesulfonic acid (PTSA), and under very low humidity conditions.[29] Additionally, the conductivities values of OPBI homopolymer are usually similar to PBI systems, as reported by Li *et al.*[13] A proton conductivity of PA-doped PBI membrane, in similar membrane preparation and conductivity measurement conditions, of 62 $mS \cdot cm^{-1}$ was found at high temperature (180 ºC). Here we obtained values at around 67 $mS \cdot cm^{-1}$ at 140 ºC for OPBI pure membranes. The main advantage of OPBI samples respect to PBI structure was discussed in the introduction section, however, compared to Nafion membranes, additionally to the high temperature application advantage, the other important concern is the cost of production, as recently stated by Singha *et al*.[20]

In summary, the high conductivity of OPBI doped pristine membranes was attributed to the good charge mobility imparted by the PA dopant. On the other hand, the utilization of

DBSA as co-dopant agent did not enhance the OPBI proton conductivity, even doped. As a main advantage, the incorporation of DBSA provides dimensional stability in comparison to OPBI films and OPBI/DBSA films show almost constant charge mobility from 22 ºC to 140 ºC. Therefore, the utilization of OPBI/DBSA (12.5 wt. %) as proton exchange membranes is appropriated for operations at such restricted temperature interval.

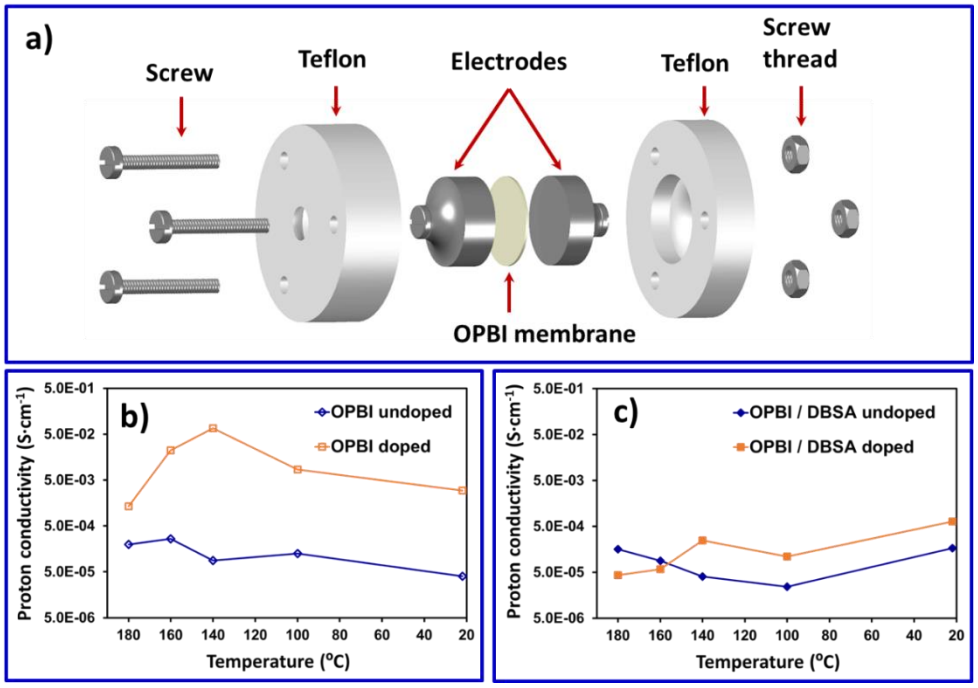

Figure 9. (a) Capacitor cell used to measure the resistance of the OPBI films. Temperature dependence of the proton conductivity for (b) OPBI and (c) OPBI/DBSA (12.5 wt. %) membranes.

Mechanism of charge mobility in OPBI/DBSA films

The good proton conductivity mechanism of phosphoric acid-doped OPBI membranes is well-known and previously reported.[3, 4] Based on the conduction pathway generated by the synergistic combination of PA dimers and water molecules, and in the interaction of PA

with OPBI matrix (Scheme 1a), we can propose one explanation for the lower conductivities achieved when DBSA molecules are used as acidic surfactant molecule, if compared to the pristine polymer. As can be seen in the Scheme 1b, the long chain of DBSA units should be the responsible to hinder the proton transfer between imidazole rings and phosphoric acid molecules. The long methylene chain in DBSA helps the flexibility of the whole system, *i.e.* films with proper handling than pristine polymer, were obtained (Figure 1); but the large carbon chain reduces the proton conduction properties (Figure 9c). When the temperature increases, the dodecyl arm is supposed to vibrate and such structural change is found to have a more negative effect on the proton conductivity, preventing the meeting of PA molecules and the polymer matrix in a strongest manner, than at low temperatures. For the mechanism elucidation, we assumed that the acid surfactant was successfully and homogenously incorporated in OPBI matrix, as proved by the characterization results reported here.

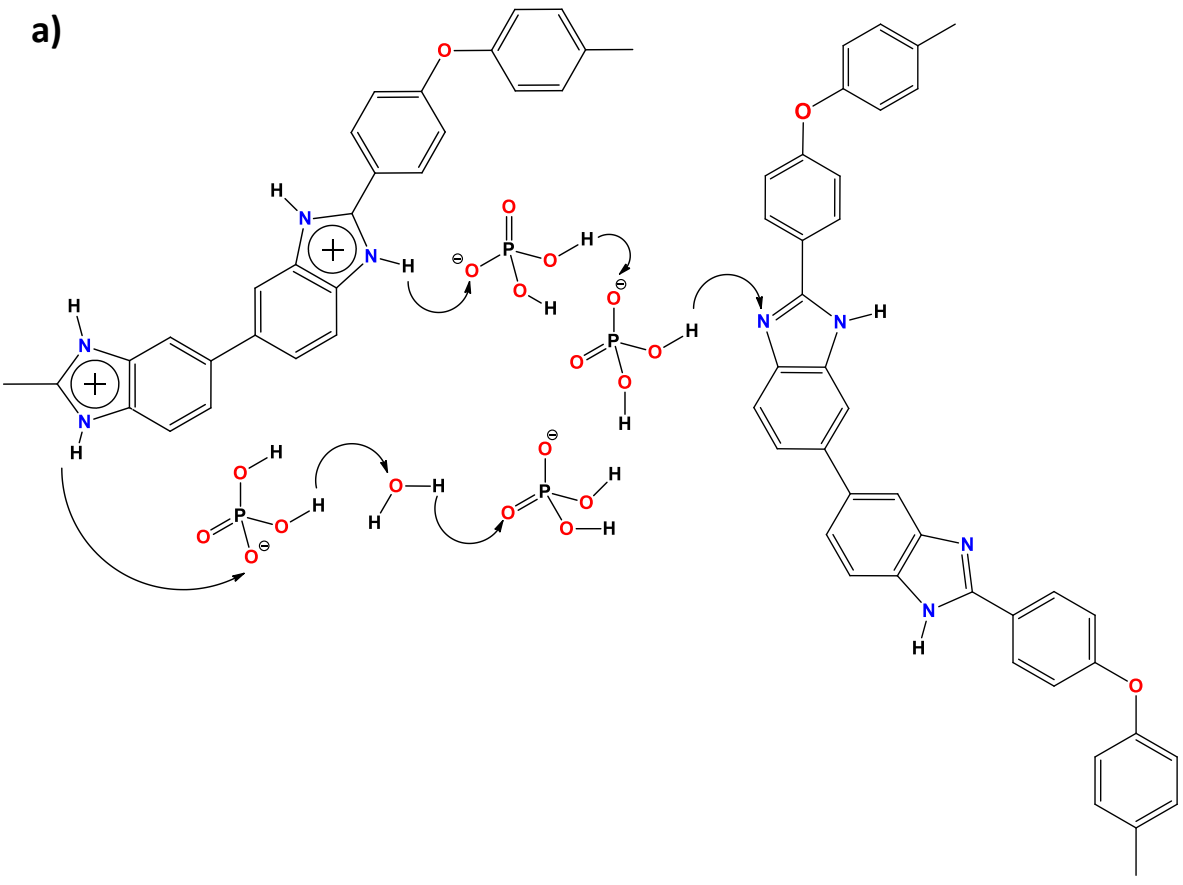

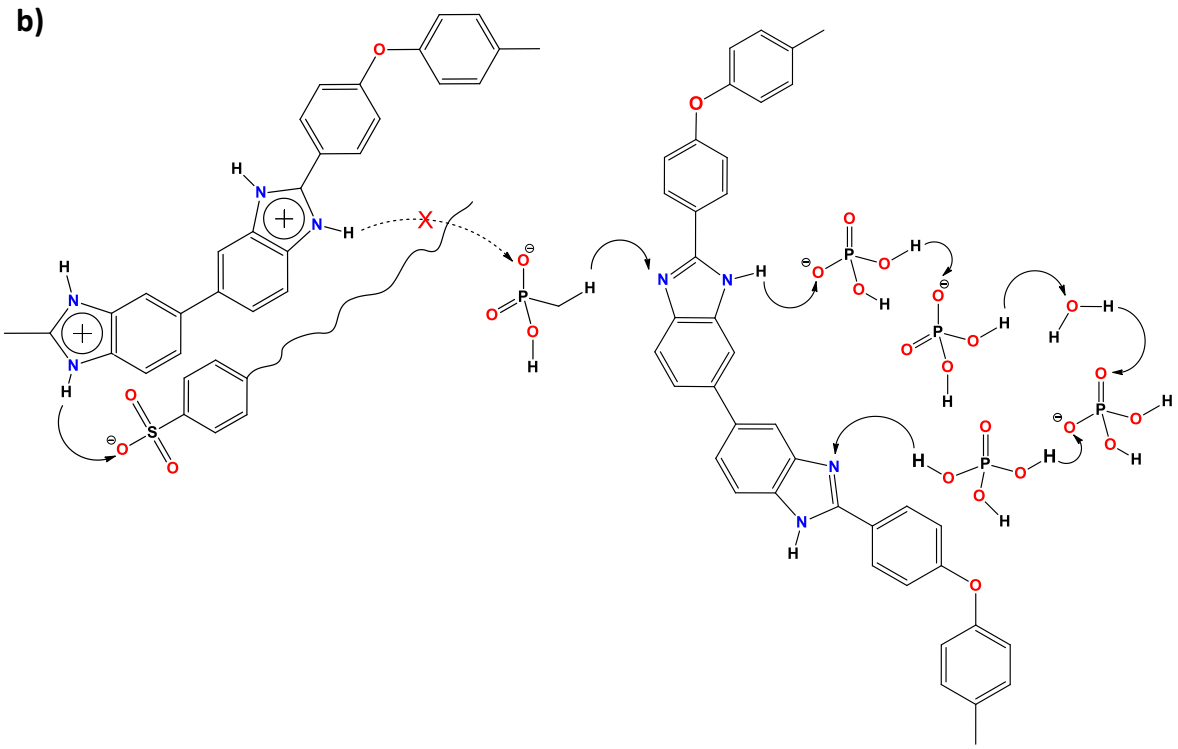

Scheme 1. (a) Proton conductivity mechanism of PA-doped OPBI membrane, and (b) proton conductivity mechanism of PA-doped OPBI membrane modified with DBSA molecules.

CONCLUSION

A sulfonic acid surfactant with long methylene groups (DBSA), at different concentrations, has been used as co-dopant and co-plasticizer agent to OPBI thermoplastic polymer. Comparison with pristine membranes showed a substantial improvement in the film handling, either for the undoped or doped OPBI/DBSA membranes, when a low content of DBSA was employed (12.5 wt.%). Moreover, the thermal stability was preserved, the brittle behavior was improved, and an excellent dimensional stability was achieved. The proton conductivity has been reduced if compared to the PA-doped OPBI films, but the charge mobility in OPBI/DBSA films remain quite stable from low to moderate temperatures. This behavior is the opposite to that usually observed for common PEMs. Above 140 ºC the DBSA additive seems to start to decompose, as suggested by the darkness color of the films after temperature stabilization, under dry conditions. Therefore, DBSA and PA molecules can be

used as complementary plasticizer agents in OPBI systems, improving the mechanical stability of the films, whereas the use of DBSA as charge mobility promoter in PEMs is limited by the temperature interval described in this work.

Supplementary information: The following are available online: Experimental procedure, Figures S1-S11; Table S1.

Acknowledgments: The authors acknowledge the financial support provided by MINECO-FEDER (RTI2018-098951-B-I00) and the Agència de Gestió d'Ajuts Universitaris i de Recerca (AGAUR, number 2017SGR359). C. A. acknowledges the Generalitat de Catalunya (Catalonia-Spain) for the distinguished prize "ICREA Academia 2015".

References

1. Li Q, Jensen JO, Savinell RF, Bjerrum NJ (2009) High temperature proton exchange membranes based on polybenzimidazoles for fuel cells. Prog Polym Sci 34:449–477. https://doi.org/10.1016/j.progpolymsci.2008.12.003
2. Peighambardoust SJ, Rowshanzamir S, Amjadi M (2010) Review of the proton exchange membranes for fuel cell applications. Elsevier Ltd
3. Asensio JA, Sánchez EM, Gómez-Romero P (2010) Proton-conducting membranes based on benzimidazole polymers for high-temperature PEM fuel cells. A chemical quest. Chem Soc Rev 39:3210–3239. https://doi.org/10.1039/b922650h
4. Subianto S (2014) Recent advances in polybenzimidazole/phosphoric acid membranes for high-temperature fuel cells. Polym Int 63:1134–1144. https://doi.org/10.1002/pi.4708

5. Haque MA, Sulong AB, Loh KS, et al (2017) Acid doped polybenzimidazoles based membrane electrode assembly for high temperature proton exchange membrane fuel cell: A review. Int J Hydrogen Energy 42:9156–9179. https://doi.org/10.1016/j.ijhydene.2016.03.086

6. Nawn G, Pace G, Lavina S, et al (2015) Nanocomposite Membranes based on Polybenzimidazole and ZrO2 for High-Temperature Proton Exchange Membrane Fuel Cells. ChemSusChem 8:1381–1393. https://doi.org/10.1002/cssc.201403049

7. Özdemir Y, Üregen N, Devrim Y (2017) Polybenzimidazole based nanocomposite membranes with enhanced proton conductivity for high temperature PEM fuel cells. Int J Hydrogen Energy 42:2648–2657. https://doi.org/10.1016/j.ijhydene.2016.04.132

8. Li Q, Aili D, Hjuler HA, Jensen JO (2016) High Temperature Polymer Electrolyte Membrane Fuel Cells. Springer International Publishing, Switzerland

9. Ellis B, Smith R (2009) Polymers : a property database. CRC Press/Taylor & Francis Group

10. Li Q, He R, Berg RW, et al (2004) Water uptake and acid doping of polybenzimidazoles as electrolyte membranes for fuel cells. Solid State Ionics 168:177–185. https://doi.org/10.1016/j.ssi.2004.02.013

11. Hwang K, Kim JH, Kim SY, Byun H (2014) Preparation of polybenzimidazole-based membranes and their potential applications in the fuel cell system. Energies 7:1721–1732. https://doi.org/10.3390/en7031721

12. Perry KA, Eisman GA, Benicewicz BC (2008) Electrochemical hydrogen pumping using a high-temperature polybenzimidazole (PBI) membrane. J Power Sources

177:478–484. https://doi.org/10.1016/j.jpowsour.2007.11.059

13. Li X, Chen X, Benicewicz BC (2013) Synthesis and properties of phenylindane-containing polybenzimidazole (PBI) for high-temperature polymer electrolyte membrane fuel cells (PEMFCs). J Power Sources 243:796–804

14. Shabani M, Younesi H, Pontié M, et al (2020) A critical review on recent proton exchange membranes applied in microbial fuel cells for renewable energy recovery. J Clean Prod 264:. https://doi.org/10.1016/j.jclepro.2020.121446

15. Aili D, Yang J, Jankova K, et al (2020) From polybenzimidazoles to polybenzimidazoliums and polybenzimidazolides. J Mater Chem A 8:12854–12886. https://doi.org/10.1039/d0ta01788d

16. Sannigrahi A, Ghosh S, Lalnuntluanga J, Jana T (2009) How the Monomer Concentration of Polymerization Influences Various Properties of Polybenzimidazole: A Case Study with Poly(4,40-diphenylether-5,50- bibenzimidazole). J Appl Polym Sci 111:2194–2203. https://doi.org/10.1002/app

17. Singha S, Jana T (2014) Structure and Properties of Polybenzimidazole/Silica Nanocomposite Electrolyte Membrane: Influence of Organic/Inorganic Interface. ACS Appl Mater Interfaces 6:21286−21296

18. Wang L, Ni J, Liu D, et al (2018) Effects of branching structures on the properties of phosphoric acid-doped polybenzimidazole as a membrane material for high-temperature proton exchange membrane fuel cells. Int J Hydrogen Energy 43:16694–16703. https://doi.org/10.1016/j.ijhydene.2018.06.181

19. He R, Li Q, Xiao G, Bjerrum NJ (2003) Proton conductivity of phosphoric acid doped

polybenzimidazole and its composites with inorganic proton conductors. J Memb Sci 226:169–184. https://doi.org/10.1016/j.memsci.2003.09.002

20. Singha S, Jana T, Modestra JA, et al (2016) Highly efficient sulfonated polybenzimidazole as a proton exchange membrane for microbial fuel cells. J Power Sources 317:143–152. https://doi.org/10.1016/j.jpowsour.2016.03.103

21. Ngamsantivongsa P, Lin HL, Yu TL (2016) Crosslinked ethyl phosphoric acid grafted polybenzimidazole and polybenzimidazole blend membranes for high-temperature proton exchange membrane fuel cells. J Polym Res 23:1–11. https://doi.org/10.1007/s10965-015-0911-3

22. Liu C, Wang X, Li Y, et al (2017) Novel cross-linked membranes based on polybenzoxazine and polybenzimidazole containing 4-phenyl phthalazinone moiety for high-temperature proton exchange membrane. J Polym Res 24:1–11. https://doi.org/10.1007/s10965-016-1173-4

23. Wang P, Liu Z, Li X, et al (2019) Toward enhanced conductivity of high-temperature proton exchange membranes: Development of novel PIM-1 reinforced PBI alloy membranes. Chem Commun 55:6491–6494. https://doi.org/10.1039/c9cc02102g

24. Li X, Ma H, Wang P, et al (2019) Construction of High-Performance, High-Temperature Proton Exchange Membranes through Incorporating SiO2 Nanoparticles into Novel Cross-linked Polybenzimidazole Networks. ACS Appl Mater Interfaces 11:30735–30746. https://doi.org/10.1021/acsami.9b06808

25. Wang L, Liu Z, Ni J, et al (2019) Preparation and investigation of block polybenzimidazole membranes with high battery performance and low phosphoric

acid doping for use in high-temperature fuel cells. J Memb Sci 572:350–357. https://doi.org/10.1016/j.memsci.2018.10.083

26. Skorikova G, Rauber D, Aili D, et al (2020) Protic ionic liquids immobilized in phosphoric acid-doped polybenzimidazole matrix enable polymer electrolyte fuel cell operation at 200 °C. J Memb Sci 608:118188. https://doi.org/10.1016/j.memsci.2020.118188

27. Cai Y, Yue Z, Jiang Q, Xu S (2018) Modified silicon carbide whisker reinforced polybenzimidazole used for high temperature proton exchange membrane. J Energy Chem 27:820–825. https://doi.org/10.1016/j.jechem.2017.05.002

28. Wang S, Sun P, Li Z, et al (2018) Comprehensive performance enhancement of polybenzimidazole based high temperature proton exchange membranes by doping with a novel intercalated proton conductor. Int J Hydrogen Energy 43:9994–10003. https://doi.org/10.1016/j.ijhydene.2018.04.089

29. Sana B, Jana T (2016) Polybenzimidazole composite with acidic surfactant like molecules: A unique approach to develop PEM for fuel cell. Eur Polym J 84:421–434. https://doi.org/10.1016/j.eurpolymj.2016.09.051

30. Murphy J (2001) Additives for Plastics Handbook, 2nd Editio. Elsevier Advanced Technology, Oxford

31. Zweifel H, Maier RD, Schiller M (2009) Plastics Additives Handbook, 6th Editio. Hanser Publications, Munich

32. Wang JTW, Hsu SLC (2011) Enhanced high-temperature polymer electrolyte membrane for fuel cells based on polybenzimidazole and ionic liquids. Electrochim

Acta 56:2842–2846. https://doi.org/10.1016/j.electacta.2010.12.069

33. Che Q, Liu L, Li Z, et al (2017) Research on methanol permeation of proton exchange membranes with incorporating ionic liquids. J Polym Res 24:1–10. https://doi.org/10.1007/s10965-017-1331-3

34. Conti F, Majerus A, Di Noto V, et al (2012) Raman study of the polybenzimidazole-phosphoric acid interactions in membranes for fuel cells. Phys Chem Chem Phys 14:10022–10026. https://doi.org/10.1039/c2cp40553a

35. Ghosh S, Maity S, Jana T (2011) Polybenzimidazole/silica nanocomposites: Organic-inorganic hybrid membranes for PEM fuel cell. J Mater Chem 21:14897–14906. https://doi.org/10.1039/c1jm12169c

36. Singha S, Jana T (2016) Influence of interfacial interactions on the properties of polybenzimidazole/clay nanocomposite electrolyte membrane. Polymer (Guildf) 98:20–31. https://doi.org/10.1016/j.polymer.2016.06.007

37. Satheesh Kumar B, Sana B, Mathew D, et al (2018) Polybenzimidazole-nanocomposite membranes: Enhanced proton conductivity with low content of amine-functionalized nanoparticles. Polymer (Guildf) 145:434–446. https://doi.org/10.1016/j.polymer.2018.04.081

38. Jayakody JRP, Chung SH, Durantino L, et al (2007) NMR Studies of Mass Transport in High-Acid-Content Fuel Cell Membranes Based on Phosphoric Acid and Polybenzimidazole. J Electrochem Soc 154:B242. https://doi.org/10.1149/1.2405726

39. Muthuraja P, Prakash S, Shanmugam VM, Manisankar P (2018) Stable nanofibrous poly(aryl sulfone ether benzimidazole) membrane with high conductivity for high

temperature PEM fuel cells. Solid State Ionics 317:201–209. https://doi.org/10.1016/j.ssi.2018.01.012

40. Mikhailenko SD, Guiver MD, Kaliaguine S (2008) Measurements of PEM conductivity by impedance spectroscopy. Solid State Ionics 179:619–624. https://doi.org/10.1016/j.ssi.2008.04.020

41. Peckham TJ, Schmeisser J, Rodgers M, Holdcroft S (2007) Main-chain, statistically sulfonated proton exchange membranes: The relationships of acid concentration and proton mobility to water content and their effect upon proton conductivity. J Mater Chem 17:3255–3268. https://doi.org/10.1039/b702339a

42. Luo X, Holdcroft S, Mani A, et al (2011) Water, proton, and oxygen transport in high IEC, short side chain PFSA ionomer membranes: Consequences of a frustrated network. Phys Chem Chem Phys 13:18055–18062. https://doi.org/10.1039/c1cp22559f

43. Yang ACC, Narimani R, Zhang Z, et al (2013) Controlling crystallinity in graft ionomers, and its effect on morphology, water sorption, and proton conductivity of graft ionomer membranes. Chem Mater 25:1935–1946. https://doi.org/10.1021/cm4005932

44. Soboleva T, Xie Z, Shi Z, et al (2008) Investigation of the through-plane impedance technique for evaluation of anisotropy of proton conducting polymer membranes. J Electroanal Chem 622:145–152. https://doi.org/10.1016/j.jelechem.2008.05.017